Journal of Applied Organometallic Chemistry

2025, Volume 5, Issue 3

Original Article

Extraction, Phytochemical Screening, Green Synthesis of Silver Nanoparticles (Ag-NPs), and Antioxidant Potential of *Aphanamixis polystachya*

P. Balaji [a] | P. Shanmugasundaram[b] | Sivabackiya Chithiravelu[c] | S. Umadevi[d,*] | Mohd Masih Uzzaman Khan[e] | I. Somasundaram[f] | Rita Dadarao Chakole[g] | Saravanan Govindaraj[h,*]

[a]*Department of Pharmacology, School of Pharmaceutical Sciences, VELS Institute of Science, Technology and Advanced Studies, Pallavaram, Chennai - 600 117, India*
[b]*Department of Pharmaceutical Chemistry and Analysis, School of Pharmaceutical sciences, Vels Institute of Science, Technology and Advanced Studies, Pallavaram, Chennai - 600 117, India*
[c]*Department of Psychiatry, SRM Medical College Hospital and Research Centre, SRMIST, SRM Nagar, Kattankulathur - 603 203. Chengalpattu District, Tamil Nadu India*
[d]*Department of Pharmaceutics, School of Pharmaceutical sciences, VELS Institute of Science, Technology and Advanced Studies, Pallavaram, Chennai - 600 117, India*
[e]*Department of Medicinal Chemistry and Pharmacognosy, College of Pharmacy, Qassim University, Buraidah 51452, Saudi Arabia*
[f]*Department of Pharmaceutics, School of Pharmaceutical Sciences, VELS Institute of Science, Technology and Advanced Studies, Pallavaram, Chennai - 600 117, India*
[g]*Department of Pharmaceutical Chemistry, Government College of Pharmacy, Osmanpura, Chhatrapati Sambhajinagar, Pin 431005, Maharashtra, India*
[h]*Department of Pharmaceutical Chemistry & Analysis, School of Pharmaceutical Sciences, Vels Institute of Science, Technology & Advanced Studies, Pallavaram, Chennai - 600 117, Tamil Nadu, India*

Use your device to scan and read the article online

Citation P. Balaji, P. Shanmugasundaram, Sivabackiya Chithiravelu, S. Umadevi, Mohd Masih Uzzaman Khan, I. Somasundaram, Rita Dadarao Chakole, Saravanan Govindaraj **Extraction, Phytochemical Screening, Green Synthesis of Silver Nanoparticles (Ag-NPs), and Antioxidant Potential of *Aphanamixis polystachya*.** *J. Appl. Organomet. Chem.*, **2025**, *5*(3), 343-367.

https://doi.org/10.48309/JAOC.2025.525464.1299

Article info:
Submitted: 2025-05-22
Revised: 2025-06-19
Accepted: 2025-07-11
ID: JAOC-2505-1299

Keywords:
Plant extracts, Ag-NPs, Spectroscopy, *A. polystachya*, Leaf extract

ABSTRACT

This study reports the green synthesis of silver nanoparticles (Ag-NPs) using an aqueous leaf extract of *Aphanamixis polystachya*, a plant known for its medicinal properties. The biosynthesized Ag-NPs were characterized using UV-Vis spectroscopy, FTIR, SEM, XRD, DLS, and zeta potential analysis. The UV-Vis spectrum displayed a surface plasmon resonance peak at 425 nm, and particle size analysis showed an optimized average diameter of 39.7 nm. Zeta potential was recorded at -9.29 mV, confirming colloidal stability, while entrapment efficiency reached 82.2%. Functional groups such as O–H, C=O, and C–N identified by FTIR analysis facilitated nanoparticle formation and stabilization. SEM revealed spherical morphology and XRD confirmed a crystalline face-centered cubic structure with peaks at 38.1°, 44.3°, 64.4°, and 77.4°. *In vitro* antioxidant evaluation using DPPH assay demonstrated superior activity of Ag-NPs (IC_{50} = 0.68 ± 0.06 mg/mL) over the crude leaf extract (IC_{50} = 1.57 ± 0.07 mg/mL). Additionally, the Ag-NPs exhibited a drug release of 98.27 ± 2.76% over 12 hours and remained physically stable over three months. These findings imply that the leaf extract of *A. polystachya* functions as a sustainable, eco-friendly, and efficient reducing and capping agent for the production of stable Ag-NPs, with encouraging prospects for additional biological and medicinal uses.

***Corresponding Authors: S. Umadevi** (umadevi.sps@vistas.ac.in) & **Saravanan Govindaraj** (sarachem1981@gmail.com)*

Introduction

The increasing demand for environmentally sustainable technologies has driven the development of green synthesis methods for nanomaterials. These approaches use biological systems such as bacteria, fungi, algae, and plants as sources of reducing and stabilizing agents, offering numerous advantages including lower toxicity, reduced environmental impact [1-3]. Cost-effectiveness, decreased pollution, and increased safety are only a few benefits of green synthesis [4].

Various nanoparticles, including metals and metal oxides for example copper oxide, zinc oxide, silver, and gold, can be produced by the procedure [1]. Applications for these green-synthesized nanomaterials are numerous and include heavy metal detection, antibacterial activity, environmental remediation, and catalysis [4]. There are still issues, though, for example restrictions on production location, time, yield, and purity [3]. Notwithstanding these limitations, green synthesis offers a viable substitute for conventional techniques, competing with the increasing focus on environmentally friendly scientific methods [2].

Ag-NPs are 1 to 100 nm-sized particles with special qualities that make them useful in various industries; for example, electronics, cosmetics, and medicine [5,6].

Physical, chemical, and biological processes can all be used to create Ag-NPs, while biological synthesis is more environmentally friendly [6]. Antibacterial, antifungal, antiviral, anti-inflammatory, and anticancer properties are among the many biological uses for these nanoparticles [7,8].

They can interface with microbial cell walls because of their tiny size, which prevents pathogen activity [7]. Compared to chemical agents, Ag-NPs have lower toxicity and antioxidant effects [7]. Their potential as photosensitizers, radio-sensitizers, and therapeutic agents for a range of malignancies such as lung, breast, and leukemia, has been investigated recently [8]. However, given their extensive use, the toxicity and environmental effects of Ag-NPs continue to be significant factors [9].

The traditional medicinal tree *Aphanamixis polystachya*, which belongs to the Meliaceae family, has shown great promise for treatment. Besides its broad pharmacological profile, *A. polystachya* is particularly suited for green synthesis of nanoparticles due to its abundance of secondary metabolites such as flavonoids, terpenoids, alkaloids, and phenolic acids which also has anti-diabetic, anti-microbial, and antioxidant qualities [10].

These phytochemicals are known to function as effective bio-reductants and capping agents in nanoparticle synthesis, aiding the conversion of silver ions (Ag^{+}) into silver nanoparticles (Ag^{+}) while simultaneously stabilizing the nanoparticles to prevent aggregation. Flavonoids and phenolics, in particular, possess hydroxyl and carbonyl functional groups that facilitate electron donation to reduce metal ions, whereas terpenoids and alkaloids contribute to nanoparticle stabilization by forming protective layers on the nanoparticle surface. This rich phytochemical composition makes *A. polystachya* an ideal candidate for the eco-friendly and bio-functional synthesis of Ag-NPs. In rats, its leaf extract shows hepatoprotective properties against liver damage caused by carbon tetrachloride [11].

To address conservation concerns, *in vitro* regeneration procedures have been devised; 3 mg/L of 2-ip produces the largest amount of biomass. Tree components and *in vitro* shoots have comparable chemical profiles, according to HPTLC analysis [12].

In India's Meerut area, great germination rates (95%) and quick growth have demonstrated the promise of conservation efforts for this endangered plant. These results demonstrate the possibility of reintroducing *A. polystachya* in regions where it is now extinct [13].

With significant DPPH, FRAP, and metal chelation effects, *A. polystachya* has robust antioxidant activity throughout its bark, leaves, and stem [13]. Its antibacterial, thrombolytic, and α-glucosidase inhibitory properties, along with its abundance of phenolics and flavonoids, support its wide range of therapeutic possibilities [14-16].

The environmentally benign, economical, and energy-efficient nature of green synthesis of Ag-NPs utilizing plant extracts has drawn a lot of attention [16]. Ag-NPs with antibacterial qualities have been created using various medicinal plants, for example *Ocimum tenuiflorum, Azadirachta indica,* and *Musa balbisiana* [17].

Plant extracts, which serve as both stabilizing and reducing agents, are used in the reduction of silver nitrate [14]. Some factors such as pH, temperature, and extract concentration influence the synthesis [15]. The nanoparticles are analyzed using characterization methods such as Fourier Transform Infrared spectroscopy (FTIR), Transmission Electron Microscopy (TEM), and UV-Visible [18].

When compared to traditional antibiotics, green-synthesized Ag-NPs had stronger antibacterial efficacy against a range of bacterial species [15, 18]. These nanoparticles also exhibit promise for environmental cleanup and agricultural uses [15]. The environmentally benign, economical, and energy-efficient method of green synthesis of Ag-NPs utilizing plant extracts has drawn significant interest [19].

Using substances produced from plants, silver ions are reduced to Ag-NPs, which are particles with a typical size range of 1 to 100 nm [20].

UV-Visible, FTIR, X-Ray Diffraction (XRD), and Scanning Electron Microscopy (SEM) are frequently used techniques for characterizing Ag-NPs [21, 22].

The synthesis process is influenced by variables for example pH, temperature, incubation duration, and quantities of silver nitrate and plant extract [19]. *A. polystachya* and other plant extracts have been used to create Ag-NPs, which have shown a range of biological activities, for example antibacterial, antioxidant, and anticancer qualities [21,22]. Ag-NPs produced from *A. polystachya*; for example, demonstrated improved antiradical potential and cytotoxic activities against cell types that cause breast cancer [21]. These green-synthesised Ag-NPs may find use in a variety of industries, for example engineering and medicine [20].

The novelty of our study lies in the use of *A. polystachya* leaf extract, unlike previous reports that utilized roots or stem bark with ethanol [16,23].

Additionally, we employed a multi-cycle cold methanolic maceration method, which enhances phytochemical yield and nanoparticle stability. This research aims to develop an eco-friendly, cost-effective method for the green synthesis of Ag-NPs using the leaf extract of *A. polystachya*, and to characterize the synthesized nanoparticles for their physicochemical properties and antioxidant potentials. The synthesized Ag-NPs will be evaluated using techniques such as UV-Visible spectroscopy, FTIR, XRD, and SEM to confirm their formation and assess their structural attributes. Antioxidant activity will be determined through assays including DPPH, FRAP, and metal chelation to establish the therapeutic potential of the nanoparticles. The green synthesis of Ag-NPs using *A. polystachya* leaf extract will be optimized by varying parameters such as pH, temperature, and extract concentration. The Ag-NPs formation will be initially confirmed through visual observation of color change and UV-Visible spectroscopy. FTIR analysis will be conducted to identify the functional groups responsible for the reduction and stabilization of silver ions. XRD patterns will be used to determine the crystalline nature and average particle size of the synthesized Ag-NPs. SEM imaging will provide data on the morphology and size distribution of the nanoparticles. The antioxidant potential of the Ag-NPs will be evaluated using DPPH free radical scavenging assay, FRAP assay, and metal chelation activity. These results will be compared with the antioxidant activity of the *A. polystachya* leaf extract alone to assess any enhancement in properties. The stability of the synthesized Ag-NPs will be evaluated over time to determine their shelf life and potential for long-term applications. The biocompatibility and cytotoxicity of the nanoparticles will be assessed using *in vitro* cell culture studies to ensure their safety for potential biomedical applications. Finally, the antibacterial activity of the Ag-NPs will be tested against common pathogenic bacteria to explore their potential as alternative antimicrobial agents.

Experimental

Materials

Identification and authentication

A. polystachya herb was collected in September 2024 from the local region of Chennai, India. From the collected plant material, the herbarium was prepared and authenticated by Dr. K. Madhava Chetty, Head of Botanical Department of Sri Venkateswara University, Tirupati, 517502, Andhra Pradesh, India. A voucher specimen no. 0101 was deposited.

Chemicals

Silver nitrate ($AgNO_3$) was used as the precursor, polyvinyl alcohol (PVA) served as the stabilizer, and sodium citrate acted as the capping agent, with deionized water employed as the solvent throughout the experiment. All organic solvents and other chemicals of analytical or chromatographic grade were procured from Loba Chemie Pvt. Ltd., Mumbai, and Merck Specialties Pvt. Ltd., Mumbai. Distilled water was used for all experimental procedures.

Methods

Plant description

Aphanamixis polystachya (Wall.) R. Parker is an evergreen, medium-sized tree belonging to the family Meliaceae. It is characterized by a straight, cylindrical trunk reaching up to 15 meters in height and 1.5-1.8 meters in diameter, along with a dense, broad crown. In traditional Sanskrit literature, the plant is known by various names, including *Anavallabha*, *Ksharayogya, Lakshmi*, *Lakshmivana*, and *Lohita* [20].

General experimental procedure

Fresh leaves of *A. polystachya* were collected, washed thoroughly with distilled water to remove debris, and shade-dried at ambient temperature. The dried leaves were then coarsely powdered using a mechanical grinder and sieved to ensure uniform particle size. A total of 500 g of powdered material was subjected to cold maceration with methanol in a conical flask for 72 hours with occasional shaking. After three days, the extract was filtered, and the process was repeated two more times with fresh solvent to ensure complete extraction. All filtrates were pooled and concentrated under reduced pressure using a rotary evaporator (Heidolph, Germany) at 40-45 °C, yielding a viscous methanolic extract. This crude extract was dried and stored in airtight containers at 4 °C for further use [21].

Evaluation parameters of powdered crude drug

Evaluation of powdered crude drugs includes determining ash value, acid-insoluble ash, water- and alcohol-soluble extractives, and pH. Ash values detect inorganic impurities and silica content, while extractive values estimate active constituents. The pH assessment helps evaluate the drug's acidity or alkalinity, affecting stability and efficacy [21].

Physical spectral characterization of extract

Phytochemical screening

The methanolic extract was subjected to standard qualitative phytochemical tests to identify the presence of major secondary metabolites such as alkaloids, flavonoids, tannins, saponins, terpenoids, and phenolics.

UV-Vis spectral analysis

The color change of the reaction mixture was visually observed, and silver ion bio-reduction was monitored by measuring UV-Vis spectra of 0.5 ml aliquots taken at intervals. The spectra were recorded at different time intervals using a UV-Vis spectrophotometer (UV-2450, Shimadzu) [22].

FTIR analysis

FTIR spectra of the extract were recorded using a Shimadzu FTIR spectrometer (Version 7.03, Japan) in the spectral range of 4000–400 cm^{-1}. Approximately 10 mg of dried sample was

mixed with spectroscopic grade KBr, pressed into a pellet, and scanned to detect characteristic functional groups [22].

Powder X-ray diffraction (PXRD)

Samples were prepared by centrifuging the leaf extract solution at 10,000 rpm for 30 minutes. The dried sample was smeared on a glass slide and analyzed using a (BRUKER AXS-D8 ADVANCE) X-ray diffractometer with CuKα radiation, scanned from 2° to 80° (2θ) at 10°/min, under 30 kV and 30 mA conditions [24].

Extract excipients compatibility study

FTIR analysis

FTIR spectra of the extract were recorded using a Shimadzu FTIR spectrometer (Version 7.03, Japan) in the spectral range of 4000–400 cm^{-1}. Approximately 10 mg of dried sample was mixed with spectroscopic grade KBr, pressed into a pellet, and scanned to detect characteristic functional groups [22].

Synthesis of Ag-NPs using leaf extracts

Silver nanoparticles were synthesized using the methanolic leaf extract of *Aphanamixis polystachya* as a reducing and capping agent. A 1 mM $AgNO_3$ solution (HiMedia, India) was prepared in deionized water, and 10 mL of plant extract (100 mg/mL) was added dropwise to 90 mL of $AgNO_3$ under magnetic stirring at ambient temperature (25 ± 2 °C). The mixture was incubated in the dark for 24 hours, and Ag-NP formation was confirmed by a color change from pale yellow to dark brown. The reaction mixture was centrifuged at 5000 rpm for 15 minutes (REMI C-24, India). The pellet was washed with deionized water and ethanol, dried at 40 °C, and stored for characterization. The supernatant was retained for further analysis [25].

Experimental design for optimization of Ag-NPs

A 3^2 level Central Composite Design (CCD) was used to evaluate the effects of $AgNO_3$ concentration (X1), extract concentration (X2), and stirring speed (X3) on particle size (Y1) and entrapment efficiency (Y2). Nanoparticles were synthesized based on the experimental design generated using Design-Expert® Software (Version 11), as indicated in **Table 1**.

Characterization of Ag-NPs

FTIR spectrophotometer study

FTIR spectroscopy was performed using a Perkin-Elmer LS-55 spectrometer in the range of 4000–400 cm^{-1}, employing the KBr pellet method. This analysis was carried out to identify the functional groups of biomolecules responsible for the reduction of Ag^+ ions and stabilization (capping) of the synthesized silver nanoparticles (Ag-NPs) [24].

Particle size, Zeta potential, and PDI analysis

Particle size, PDI, and zeta potential were measured using dynamic light scattering (Nanosizer 90ZS, Malvern Instruments). Samples were diluted with double distilled water and analyzed at 25 °C using 10 mm polystyrene cells at a 90° angle. Zeta potential was determined via electrophoretic mobility, and average values were calculated for the optimized batch [25].

Entrapment efficiency (%EE)

Entrapment efficiency (%EE) was calculated using the following formulas:
EE = (Total drug – Un-entrapped drug) × 100 / Total drug [25].

Table 1 (A). Independent variables values for central composite design

Independent Variables Coded Values	Low (-)	High (+)
X1: Concentration of $AgNO_3$ (mM)	1	3
X2: Concentration of Extract (gm)	0.5	1.5
X3: Stirring Speed (RPM)	150	250

Scanning electron microscopy (SEM)

The morphology of Ag-NPs was examined using a PHILIPS CM-200 scanning transmission microscope (20-200 kV, 2.4 *Å* resolution). SEM images, formed by transmitted electrons, provide magnifications up to 1,000,000X with resolution below 10 *Å* [25].

PXRD

Samples were smeared on glass slides and analyzed by PXRD using a (BRUKER AXS-D8 ADVANCE) with CuKα radiation (2°–80° 2θ), at 30 kV, 30 mA, and a scan rate of 10°/min. Ag-NPs aqueous solutions were prepared by centrifugation at 10,000 rpm for 30 minutes [24].

In vitro drug release study

The in-vitro release of *A. polystachya*-loaded Ag-NPs were studied using the dialysis bag diffusion method with a membrane (MWCO 12,000–14,000 kD) pre-activated in boiling water. Ag-NPs were sealed in the membrane and immersed in 100 ml phosphate buffer (pH 7.4) stirred at 100 rpm. Samples (2 ml) were taken at set intervals (0, 2, 4, 6, 10, 12 hrs), replaced with fresh buffer, and analyzed by UV-Vis spectrophotometry [24,25].

Accelerated stress stability study

Stability studies of the optimized APNP were conducted for 3 months following ICH guidelines. Samples stored in amber glass bottles were kept at 40±5 °C and 70%±5% RH, then tested for %EE, particle size, and PDI [24,25].

Antioxidant activity (DPPH)

The antioxidant activity of Ag-NPs and the aqueous leaf extract was assessed using the DPPH assay. Different extract concentrations (0.2-1 mg/mL) were mixed with 3 mL of 0.1 mM methanolic DPPH and incubated for 30 minutes. Absorbance was measured at 517 nm, and radical scavenging (%) was calculated as [(Ao – Ae)/Ao] × 100. Results were reported as IC_{50}, the concentration needed to inhibit 50% of DPPH radicals [25].

Results and Discussion

Evaluation parameters of powdered crude drug

The powdered crude leaf extract of *A. polystachya* was evaluated for its physical parameters. The powder appeared light brownish green in color and possessed a characteristic odor. The total ash value was found to be 3.82%, while the acid-insoluble ash value was 0.84%, indicating a low level of inorganic impurities. The water-soluble extractive value was recorded as 12.46%, and the alcohol-soluble extractive value was 6.21%, reflecting the presence of polar and semi-polar phytoconstituents. No foreign matter was detected in the sample, indicating good quality and purity. The pH of a 1% aqueous solution of the powdered extract was found to be 6.2, suggesting a slightly acidic to neutral nature as shown in **Table 1**.

Table 1. Physical parameters of powdered crude drug

Sr./ No.	Parameters	*A. polystachya*
1	Colour	Light brownish Green
2	Odour	Characteristic
3	Ash Value (%)	3.82%
4	Acid- Insoluble ash value (%)	0.84%
5	Water- soluble extractive value (%)	12.46%
6	Alcohol-soluble extractive value (%)	6.21%
7	Foreign matter	Nil
8	PH	6.2

Physical characterization and identification of extract

Phytochemical screening

Preliminary phytochemical screening of the sample revealed a diverse array of bioactive compounds (**Table 2**).

The analysis confirmed the presence of alkaloids, which are nitrogen-containing organic compounds known for their pharmacological effects. Carbohydrates, essential energy sources and structural components, were also detected. The sample contained triterpenoids and steroids, both classes of lipids with potential medicinal properties. Tannins and phenolics, compounds often associated with antioxidant activity, were identified. The presence of proteins, fundamental building blocks of cellular structures, was noted. Additionally, glycosides, compounds consisting of a sugar molecule bound to a non-sugar moiety, were detected. Interestingly, the analysis showed the absence of starch, a complex carbohydrate commonly found in plant materials. This comprehensive phytochemical profile provides valuable insights into the potential biological activities and therapeutic applications of the sample, warranting further investigation into its medicinal properties and possible uses in various fields such as pharmaceuticals, nutraceuticals, or cosmeceuticals.

UV-vis spectral analysis

The UV-Vis spectral analysis of the leaf extract from *A. polystachya* revealed a distinctive absorption peak at approximately 430 nm, as illustrated in **Figure 1**.

Table 2. Preliminary phytochemical screening of the sample

Sr./ No.	Identifications Test	Result
1	Alkaloids	Present
2	Carbohydrates	
3	Triterpenoid and Steroids	
4	Tannins and Phenolic Compounds	
5	Proteins	
6	Glycosides	
7	Starch	Absent

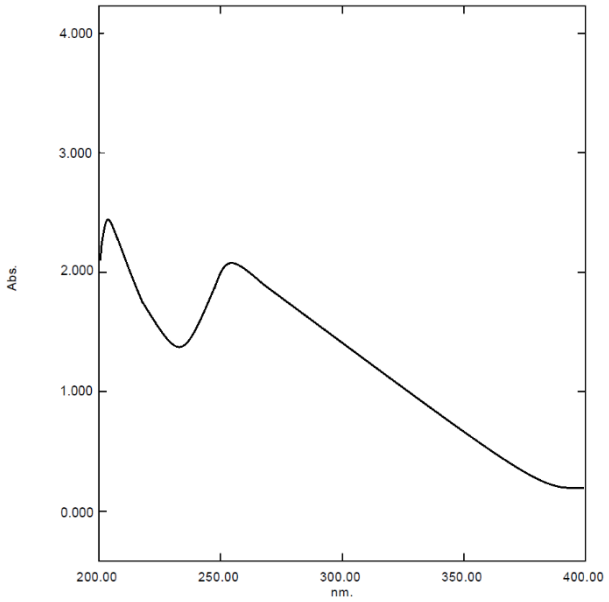

Figure 1. UV-Vis spectral analysis graph of the leaf extract from *A. polystachya* (430 nm)

This characteristic peak provides valuable information about the extract's composition and optical properties. The wavelength of 430 nm falls within the visible spectrum, corresponding to the blue-violet region, which suggests the presence of compounds that absorb light in this range. Such compounds may include various pigments, flavonoids, or other phytochemicals commonly found in plant extracts. The observation of this peak not only confirms the presence of specific light-absorbing molecules, but also serves as a potential fingerprint for identifying and characterizing the leaf extract of *A. polystachya*. Further analysis of the UV-Vis spectrum, including the examination of additional peaks or shoulders, could provide more comprehensive insights into the chemical profile and potential bioactive components of the extract.

FTIR analysis

In **Figure 2 (A)**, the FTIR spectral analysis of *A. polystachya* leaf extract revealed the presence of key functional groups associated with its phytochemical constituents. A broad vibrational band around ~3430 cm^{-1} corresponded to the stretching vibrations of hydroxyl (O–H) groups, suggesting the presence of alcohols or phenolic compounds primarily from polyphenols and flavonoids (e.g., quercetin and kaempferol). Characteristic peaks observed at 1730 cm^{-1} were attributed to the stretching vibrations of carbonyl (C=O) functional groups, indicating esters or carboxylic acids. Additional peaks around 2926 cm^{-1} and 2854 cm^{-1} were associated with asymmetric and symmetric C–H stretching vibrations of methylene (CH_2) groups, primarily from phospholipids.
A distinct peak observed at 1635 cm^{-1} was assigned to the C=O stretching vibrations, further confirming the presence of carbonyl functionalities from flavonoids and tannins. The similarity of the spectral features with the reference standard validates the identity of the phytoconstituents and confirms that there are no unexpected chemical modifications, thereby justifying the use of this extract in further applications.
We have effectively identified the presence of major bioactive classes (e.g., flavonoids, phenolics, and terpenoids) through preliminary phytochemical screening and FTIR analysis. The FTIR spectra revealed:
A broad absorption band near 3430 cm^{-1}, corresponding to –OH stretching vibrations, indicative of phenolics and flavonoids. Sharp peaks around 1730 cm^{-1} and 1635 cm^{-1} related to C=O stretching, typical of carbonyl compounds such as flavonoids and tannins. Additional bands at 2926 cm^{-1} and 2854 cm^{-1} suggest C–H stretching from terpenoids. A peak near 1384 cm^{-1} corresponds to C–N stretching, supporting the presence of alkaloids and glycosidic structures. These assignments are consistent with previous reports on plant-based nanoparticle synthesis where FTIR was used to identify key reducing agents [26-28].

PXRD study

X-ray powder diffraction (XRD) analysis is a powerful and widely used technique for characterizing the structural properties of crystalline materials. This non-destructive method provides valuable insights into the phase composition, molecular arrangement, and degree of crystallinity in a sample. The XRD pattern of the extract revealed several distinct sharp peaks at specific 2θ values, including 5.896°, 13.521°, 18.061°, 19.511°, 22.215°, and 23.255°, as displayed in **Figure 2(B)**.
The presence of these well-defined peaks is a strong indication of a highly ordered crystalline structure within the sample. The sharpness and intensity of these peaks suggest a high degree of crystallinity, while their positions correspond to specific inter-planar spacings within the crystal lattice. This information can be used to identify the crystalline phases present, estimate crystallite size, and determine the overall crystallinity of the material.
Furthermore, the absence of a broad amorphous halo in the XRD pattern suggests that the sample contains minimal or no amorphous content. The data obtained from this XRD analysis can be further utilized for quantitative phase analysis, structural refinement, and comparison with known crystalline structures to elucidate the precise molecular arrangement of the extract.

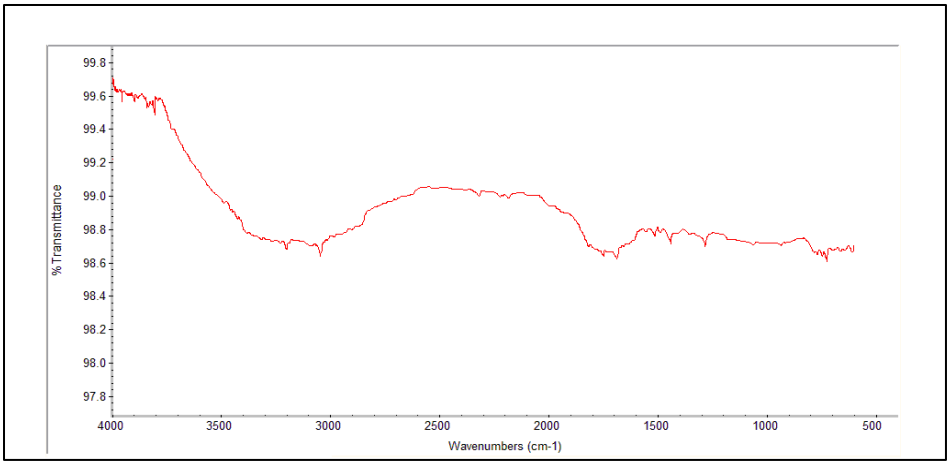

Figure 2 (A). FTIR spectra of *A. polystachya* leaf extract

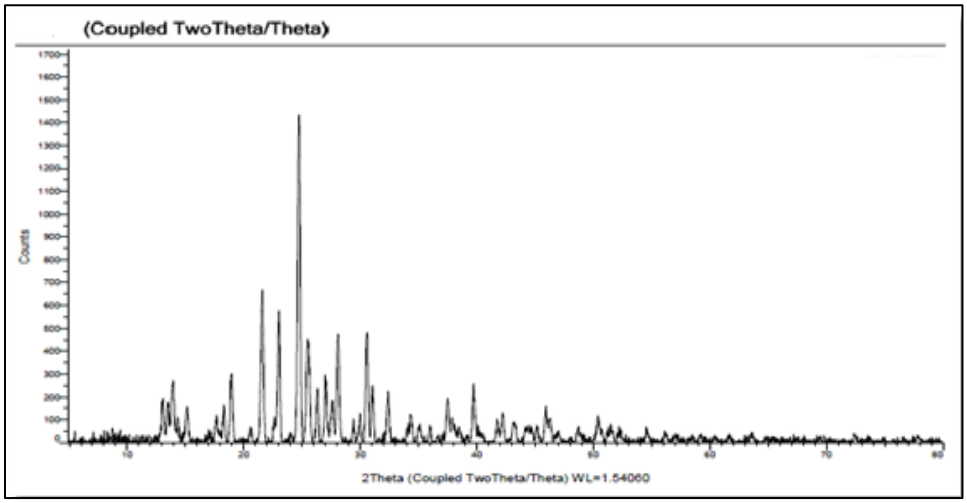

Figure 2 (B). XRD spectra of *A. polystachya* leaf extract

Extract-excipients compatibility study

FTIR analysis

In **Figures 2(A)- 4(A and B)**, the FTIR spectra of *A. polystachya* extract and the physical mixture containing all excipients (including silver nitrate and PVA) display characteristic peaks that are comparable to the reference standard. A broad vibrational band around ~3430 cm^{-1} corresponded to the stretching vibrations of hydroxyl (O–H) groups, suggesting the presence of alcohols or phenolic compounds primarily from polyphenols and flavonoids (e.g., quercetin and kaempferol). Characteristic peaks observed at 1730 cm^{-1} were attributed to the stretching vibrations of carbonyl (C=O) functional groups, indicating esters or carboxylic acids. Additional peaks around 2926 cm^{-1} and 2854 cm^{-1} were associated with asymmetric and symmetric C–H stretching vibrations of methylene (CH_2) groups, primarily from phospholipids. A distinct peak observed at 1635 cm^{-1} was assigned to the C=O stretching vibrations, further confirming the presence of carbonyl functionalities from flavonoids and tannins. Notably, these peaks remain unaltered in the physical mixture compared to the pure extract, suggesting that there is no significant interaction between the nanoparticle (NP) and the excipients, and confirming the NP compatibility with the other formulation components.

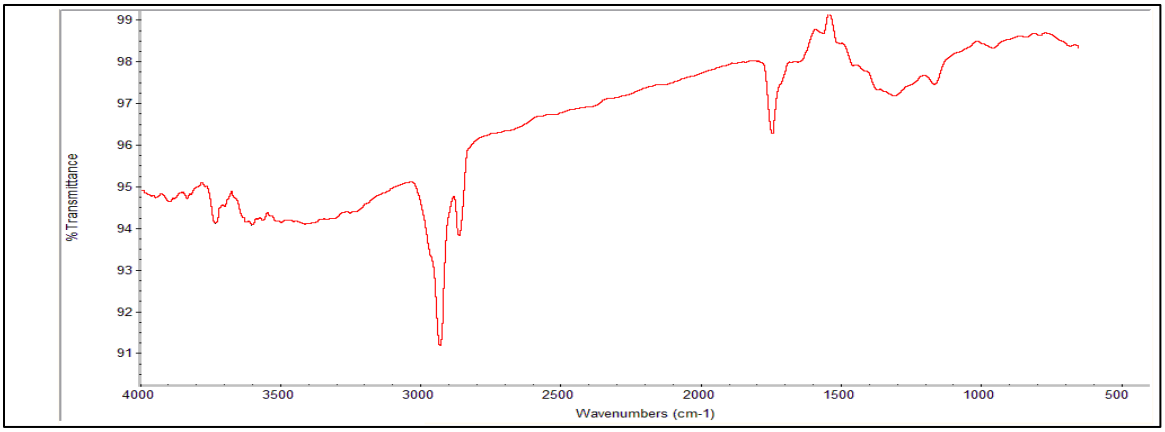

Figure 3. FTIR spectra of silver nitrate

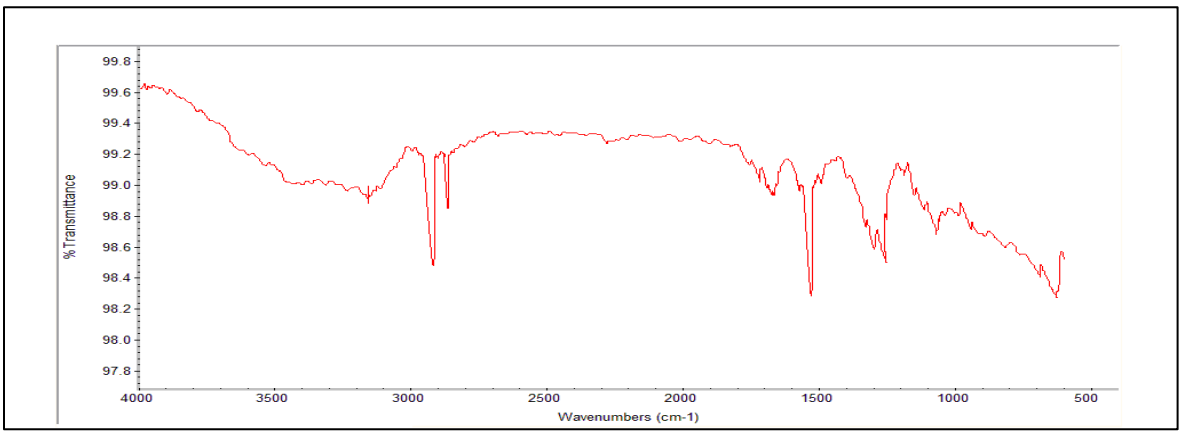

Figure 4 (A). FTIR spectra of PVA

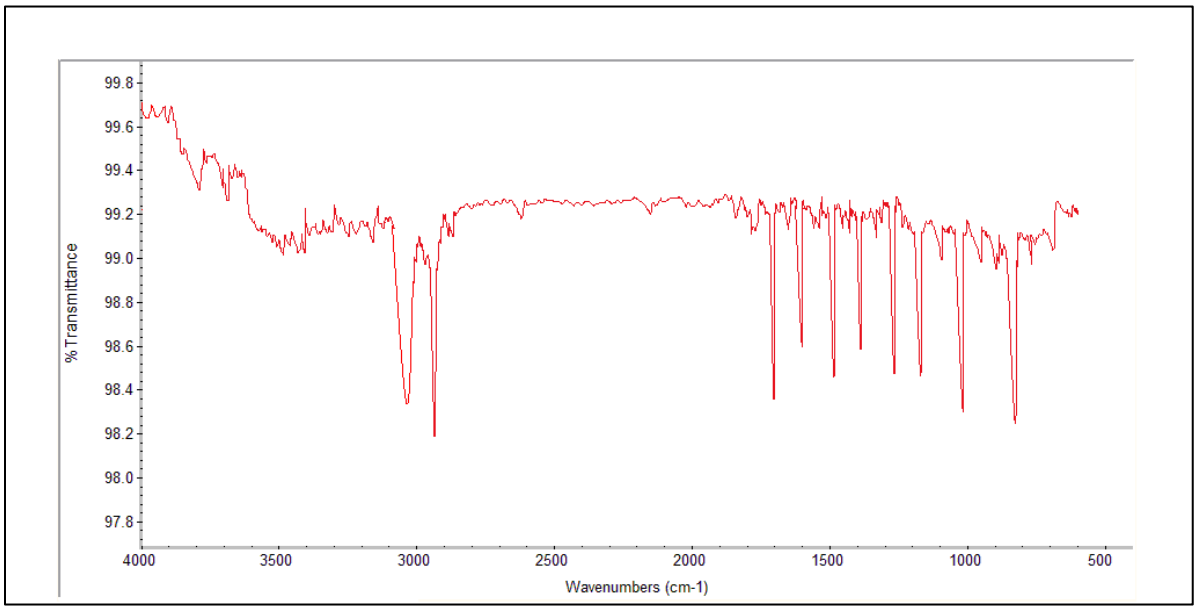

Figure 4 (B). FTIR spectra of *A. polystachya* extract and physical mixture

Formulation and selection of Ag-NPs

$AgNO_3$ is widely used as a precursor in the green synthesis of herbal Ag-NPs due to its high water solubility and efficient release of silver ions (Ag^+), which are essential for nanoparticle formation. These Ag^+ ions are readily reduced to metallic silver (Ag^0) by phytochemicals present in herbal extracts, for example, flavonoids, polyphenols, and terpenoids. $AgNO_3$ is also a stable and commercially available compound with high purity, ensuring reproducibility and consistency in nanoparticle synthesis. Its use supports eco-friendly and sustainable green synthesis methods by eliminating the need for hazardous reducing agents. Moreover, the $AgNO_3$ solubility allows for better control over the rate of Ag^+ ion release, facilitating regulation of the size, shape, and uniformity of the resulting nanoparticles.
Based on visual observations of transparency and viscosity, 20 formulations were selected using factorial design for herbal Ag-NP preparation.

Formulation design

The Central Composite Design (CCD) was employed to optimize the formulation of AgNPs using plant extract (**Table 3**). The design consisted of 20 experimental runs with varying levels of three independent variables: $AgNO_3$ concentration (X1), extract concentration (X2), and stirring speed (X3). The responses measured were particle size (Y1) and entrapment efficiency (Y2). The results showed a wide range of particle sizes, from 39.7 nm to 90.3 nm, and entrapment efficiencies ranging from 52.9% to 88%.
The data revealed that all three independent variables significantly influenced both responses. Lower $AgNO_3$ concentrations generally resulted in larger particle sizes, while higher extract concentrations tended to increase entrapment efficiency. Stirring speed showed a complex relationship with both responses, suggesting an optimal range for achieving desired particle characteristics.
Formulation F4, with 2 mM $AgNO_3$, 1.5 g extract, and 200 RPM stirring speed, yielded the smallest particle size of 39.7 nm and a high entrapment efficiency of 82.2%. This formulation represents an optimal balance between the variables, producing nanoparticles with desirable characteristics for potential applications.

Table 3. Design batches of CCD with optimized formulations using *A. polystachya* extract

Formulation Code	X1 (mM)	X2 (g)	X3 (RPM)	Y1 (nm)	Y2 (%)
F1	1.5	1	150	90.3	84.6
F2	2	0.5	200	45.8	69.1
F3	1.5	1	150	88.6	87.8
F4	**2**	**1.5**	**200**	**39.7**	**82.2**
F5	0.6591	1	150	82.4	60.9
F6	1.5	1	150	90.1	86.5
F7	1.5	1	150	58.4	74.3
F8	1.5	1	150	58.2	74.7
F9	2.3409	1	150	41.4	77.5
F10	2	1.5	100	52.7	79.6
F11	1.5	1	65.91	67	70
F12	1	1.5	200	49.1	80.2
F13	1	0.5	200	61.6	68.3
F14	2	0.5	100	60.5	65.3
F15	1	0.5	100	68.2	64.8
F16	1	1.5	100	60.6	75.5
F17	1.5	1	234.09	39.9	85.3
F18	1.5	1.8409	150	48.3	88
F19	1.5	1	150	58.5	74.4
F20	1.5	0.1591	150	75.1	52.9

The small particle size ensures a high surface area-to-volume ratio, which is crucial for many nanoparticle applications, while high entrapment efficiency indicates effective incorporation of the active components from the plant extract [29].

Optimization data analysis and model-validation

Fitting of data to model

Table 4 shows the coded and actual values of the three factors. Response ranges for Y1 (particle size) and Y2 (entrapment efficiency) were 39.7-90.7 d.nm and 52.9-88.0%, respectively. A linear model best fit the data, with R^2, adjusted R^2, predicted R^2, SD, and %CV values provided. ANOVA results (**Tables 5** and **6(A)**) confirmed model significance. Variables X1 ($AgNO_3$ concentration) and X3 (stirring speed) positively influenced entrapment efficiency and particle size optimization.

Regression Equations:

$Y1= +61.82-8.04^{*}A-5.79^{*}B-6.69^{*}C$ (3)

$Y2= +7509+2.59^{*}A+7.98^{*}B+2.95^{*}C$ (4)

Model assessment for dependent variables

The Design Expert software suggested a linear model for all responses, and statistical analysis was performed using Analysis of Variance (ANOVA). The results are presented in **Tables 5** and **6(A)**. The presence of interaction terms in the regression equations indicates that the relationship between factors and responses may vary when multiple factors change simultaneously at different levels. For the measured response Y1, the ANOVA results (**Table 5**) show that the model is significant (p-value = 0.0475).

The concentration of $AgNO_3$ (Factor A) has the most substantial effect on Y1, with an F-value of 4.47 and a p-value of 0.0505, which is borderline significant. The stirring speed (Factor C) shows some influence (F-value = 3.10, p-value = 0.0973), while the concentration of extract (Factor B) has a lesser impact (F-value = 2.32, p-value = 0.1471). The lack of fit is not significant (p-value = 0.8300), indicating that the model adequately fits the data. For the measured response Y2, the ANOVA results (**Table 6A**) demonstrate a highly significant model (p-value = 0.0013).

The concentration of extract (Factor B) has the most significant effect on Y2, with a high F-value of 20.49 and a very low p-value of 0.0003. The stirring speed (Factor C) shows some influence (F-value = 2.80, p-value = 0.1135), while the concentration of $AgNO_3$ (Factor A) has a lesser impact (F-value = 2.15, p-value = 0.1620).

The lack of fit is not significant (p-value = 0.5485), suggesting that the model adequately describes the relationship between the factors and response Y2. These ANOVA results provide valuable insights into the relative importance of each factor on the responses Y1 and Y2. The significant models and non-significant lack of fit for both responses indicate that the linear models are appropriate for describing the relationships between the factors and responses in this experimental design.

Table 4. Summary of results of regression analysis for responses Y1 and Y2

Models	R^2	Adjusted R^2	Predicted R^2	SD	%CV
Response (Y1) Linear	0.3822	0.2663	0.2001	14.04	22.71
Response (Y2) Linear	0.6139	0.5415	0.4503	6.52	8.68

Table 5. Results of analysis of variance for measured response Y1 (ANOVA)

Source	Sum of Squares	df	Mean Square	F-value	*P*-value	
Model	1951.25	3	650.42	3.30	0.0475	Significant
A-Concentration of AgNO3	882.04	1	882.04	4.47	0.0505	
B-Concentration of Extract	457.82	1	457.82	2.32	0.1471	
C-Stirring Speed	611.39	1	611.39	3.10	0.0973	
Residual	3154.48	16	197.16			
Lack of Fit	1683.18	11	153.02	0.5200	0.8300	Not Significant
Pure Error	1471.31	5	294.26			
Cor Total	5105.73	19				

Table 6(A). Results of analysis of variance for measured response Y2 (ANOVA)

Source	Sum of Squares	df	Mean Square	F-value	*P*-value	
Model	1080.90	3	360.30	8.48	0.0013	Significant
A-Concentration of AgNO3	91.33	1	91.33	2.15	0.1620	
B-Concentration of Extract	870.46	1	870.46	20.49	0.0003	
C-Stirring Speed	119.11	1	119.11	2.80	0.1135	
Residual	679.79	16	42.49			
Lack of Fit	464.48	11	42.23	0.9806	0.5485	Not Significant
Pure Error	215.31	5	43.06			
Cor. Total	1760.69	19				

3D surface plot analysis

The 3D surface plots generated by Design Expert software (**Figures 5** and **6**) provide a comprehensive visualization of the complex relationships between the formulation variables and the key response parameters: particle size (Y1) and entrapment efficiency (Y2). These plots offer valuable insights into the multifaceted interactions among silver nitrate concentration, extract quantity, and stirring speed, enabling a more nuanced understanding of their combined effects on nanoparticle characteristics. The analysis revealed that Formulation F4, characterized by 2 mM $AgNO_3$, 1.5 g extract, and 200 RPM stirring, emerged as the optimal formulation. This combination yielded nanoparticles with the smallest average particle size of 39.7 nm, which is particularly desirable for enhanced bioavailability and cellular uptake. Simultaneously, F4 demonstrated a high entrapment efficiency of 82.2%, indicating excellent incorporation of the active components within the nanoparticle structure.

Figure 6 demonstrates the 3D surface plot for the effect of $AgNO_3$ concentration (X1) and extract concentration (X2) on entrapment Efficiency (Y2). The plot shows a positive linear trend, indicating that an increase in $AgNO_3$ concentration results in enhanced entrapment efficiency. This is likely due to greater availability of reducing/stabilizing agents, allowing more efficient entrapment of Ag-NPs.
Figures 7 and **8** show the contour plots for Mean Particle Size and Entrapment Efficiency, respectively. These plots further support an increase in stirring speed and appropriate polymer-to-extract ratio, which improves nanoparticle characteristics by reducing particle size and increasing drug entrapment. An increase in stirring speed or average stirring speed enhances entrapment efficiency by increasing system viscosity, which reduces droplet size during nanoparticle formation. This contributes to smaller particles and greater entrapment due to better polymer dispersion. These findings are validated by the contour plots.

Optimisation of result

Optimization was conducted using response surface methodology with both numerical and graphical optimization tools. The desirability function was used to combine multiple goals into a single score ranging from 0 (undesirable) to 1 (ideal). The 3D surface plot for X1 ($AgNO_3$ concentration) and X3 (stirring speed) on mean particle size revealed that higher $AgNO_3$ levels led to smaller nanoparticles because of better reduction kinetics, and intermediate stirring speeds (200 RPM) produced the smallest sizes. However, optimization required consideration of both responses (Y1 and Y2).
When considering entrapment efficiency, formulations F4 and F18 showed higher values (82.2% and 88.0%, respectively), but F4 also demonstrated the smallest particle size (39.7 nm). Concerning criteria, minimum particle size and maximum entrapment efficiency; Formulation F4 was identified as the optimized batch (**Table 6B**).

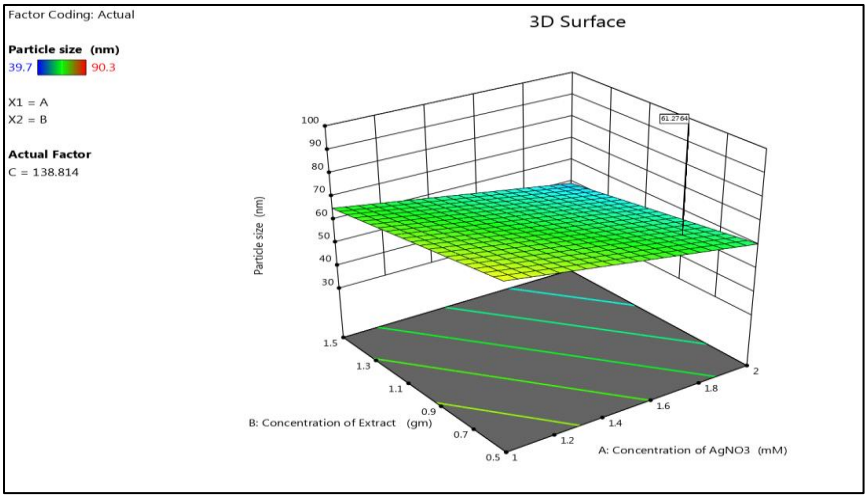

Figure 5. 3D surface plots for X1 and X2 on mean particle size (Y1)

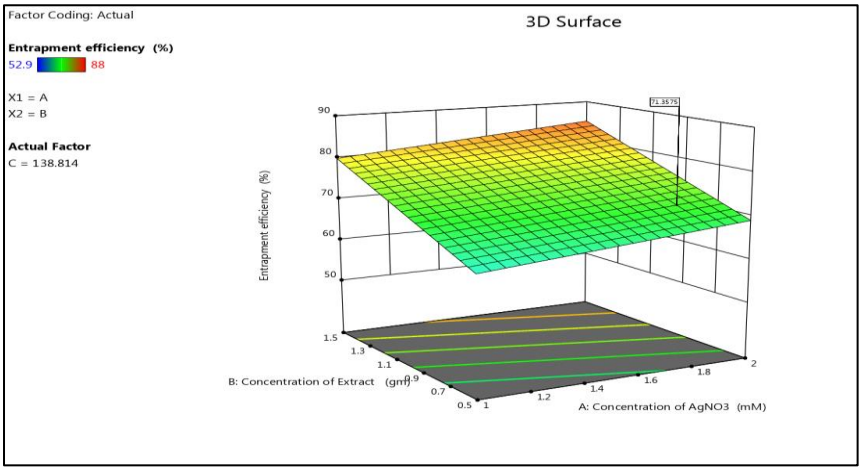

Figure 6. 3D surface plots for X1 and X2 on entrapment efficiency (Y2)

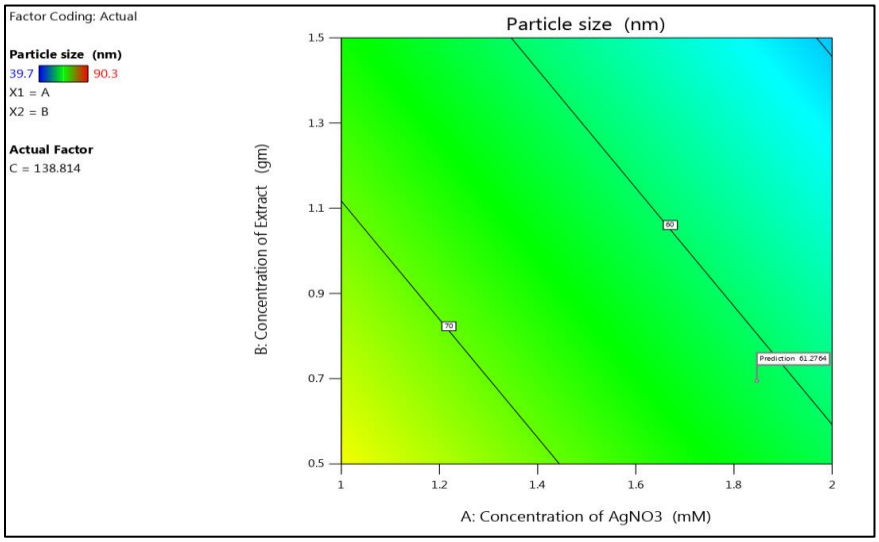

Figure 7. Contour plot of particle size (Y1)

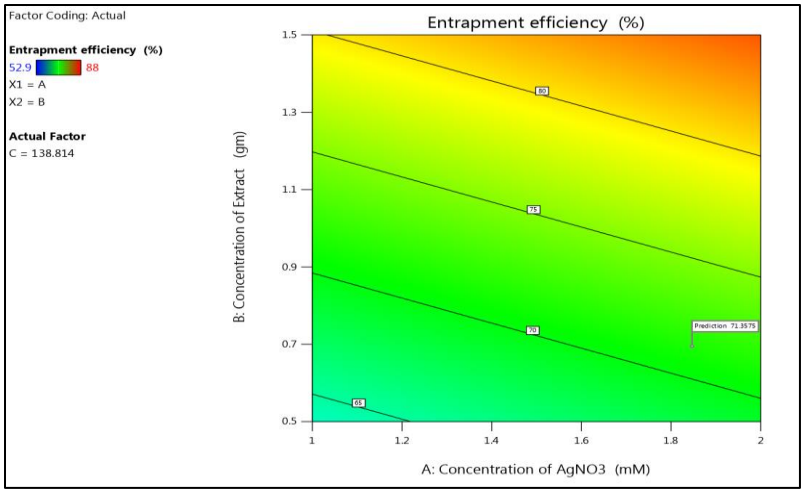

Figure 8. Contour plot of entrapment efficiency (Y2)

Table 6(B). Formulation F4 as optimized formulation batch

Sr./ No.	Ingredients	Quantity
1	Extract	1.5 gram
2	$AgNO_3$	2Mh
3	Stirring Speed	200 RPM

Characterization of Ag-NPs

FTIR spectrophotometer study

The FTIR analysis of the optimized AgNPs formulation, including the *A. polystachya* extract and excipients (for example $AgNO_3$ and PVA), revealed characteristic peaks that indicate the presence of key functional groups without significant chemical interactions between components as illustrated in **Figure 9**. A broad vibrational band around ~3430 cm^{-1} corresponded to the stretching vibrations of hydroxyl (O–H) groups, suggesting the presence of alcohols or phenolic compounds primarily from polyphenols and flavonoids (e.g., quercetin, kaempferol). Peaks at ~2926 cm^{-1} and ~2854 cm^{-1} are attributed to the asymmetric and symmetric C–H stretching of methylene ($-CH_2-$) groups, typically associated with organic compounds or excipients. The strong absorption band at ~1730 cm^{-1} indicates C=O stretching vibrations, characteristic of esters or carboxylic acids, A distinct peak observed at 1635 cm^{-1} was assigned to the C=O stretching vibrations, further confirming the presence of carbonyl functionalities from flavonoids and tannins, as shown in **Figure 9**. Other peaks at ~1384 cm^{-1} (C–N stretching of amines) and ~1052 cm^{-1} (C–O stretching of alcohols) suggest the involvement of terpenoids and glycosides in nanoparticle formation. Notably, the peak positions in the physical mixture remained unchanged compared to the pure extract, indicating no new bond formation or significant interaction, thereby confirming the chemical compatibility and stability of the nanoparticle formulation.

Particle size, Zeta potential, and PDI analysis

Particle size is analyzed using zeta-sizer and the average particle size was found to be 39.7 nm for AgNP-F4. The particle size of nanoparticles is a critical factor affecting their performance in biomedical applications, as it directly influences tissue penetration, bioavailability, and the stability of the formulation. In the provided dataset, particle sizes range from 39.7 nm to 90.7 nm. Formulation F4, with a particle size of 39.7 nm, is considered optimized because its size is sufficiently small to promote effective tissue penetration and cellular interaction, while also ensuring stability and controlled release of the therapeutic agents as shown in **Figure 10**. Zeta potential measured was found to be -9.29 mV for AgNP-F4, as demonstrated in **Figure 11**. These values indicate the Ag-NPs stabilization.

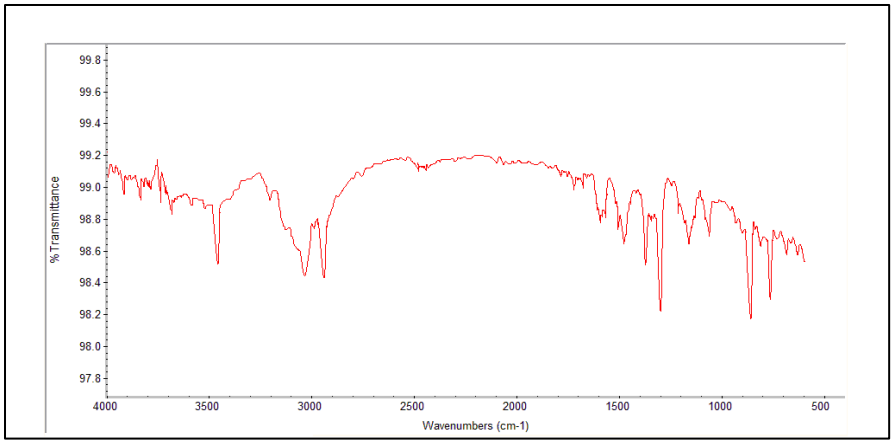

Figure 9. FTIR spectra of silver nanoparticles functionalized with *A. polystachya* extract (F4)

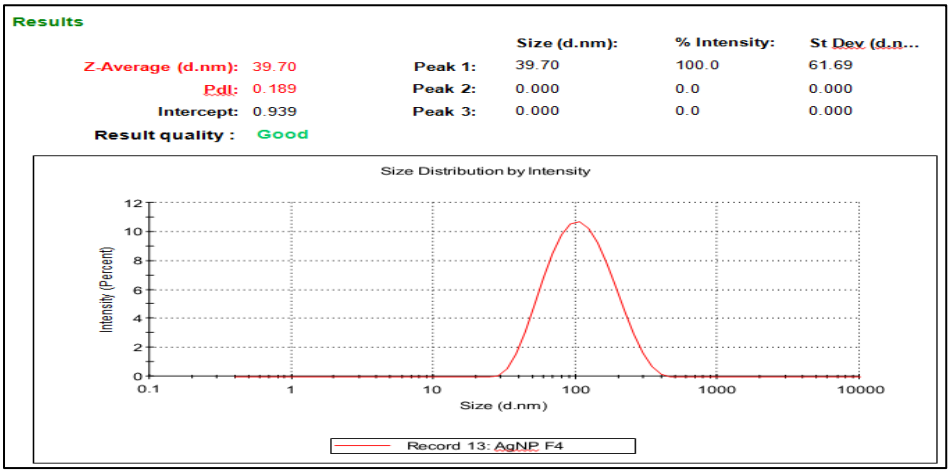

Figure 10. Particle size of F4 Ag-NP formulation

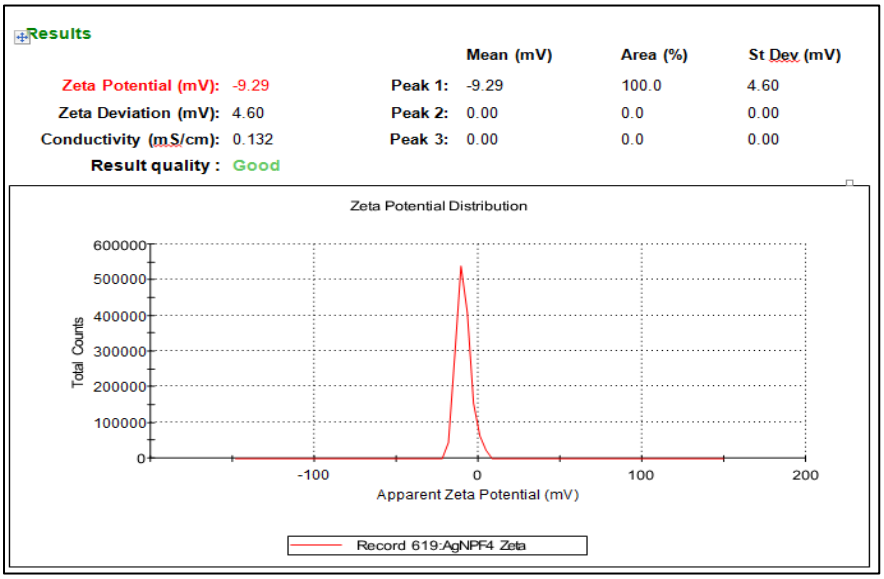

Figure 11. Zeta potential of F4 Ag-NP formulation

Entrapment efficiency (%EE)

The %EE of different formulation batches is a crucial parameter for evaluating the effectiveness of drug delivery systems. As indicated in **Table 7**, the %EE values vary significantly across the 20 formulation batches, ranging from 52.9% to 87.8%. The highest entrapment efficiency was observed in F3 (87.8%), followed closely by F17 (85.3%) and F1 (84.6%). These formulations demonstrate superior ability to encapsulate the active ingredient within the delivery system. In contrast, F20 exhibited the lowest %EE at 52.9%, indicating less effective entrapment. F4, with an entrapment efficiency of 82.2%, represents a notable improvement over many other formulations. This enhanced performance can be attributed to optimized processing conditions, particularly the combination of higher stirring speed and increased sonication time. These factors contribute to the reduction of particle size through increased shear forces and cavitation effects. The smaller particle size, coupled with the increased viscosity of the formulation, limits the diffusion of the active ingredient during the preparation process. This results in the formation of smaller droplets with a higher surface area-to-volume ratio, ultimately leading to improved entrapment of the drug within the delivery system. The superior %EE of F4 suggests that it may be a promising candidate for further development and optimization in drug delivery applications. The optimized Ag-NP formulation using *Aphanamixis polystachya* leaf extract (F4) demonstrated a high %EE (82.2%) and a small particle size (39.7 nm), as an indicative of effective capping and stabilization compared to previously reported green synthesis methods. *Acalypha indica* leaf extract synthesized Ag-NPs with particle sizes ranging from 20 to 30 nm, but reported no entrapment data, limiting direct comparison on drug-loading potential [30]. *Olea europaea* leaf extract-based Ag-NPs showed particle sizes of 20-25 nm and IC_{50} values around 1.12 mg/mL [31], while the current study achieved superior antioxidant efficacy with an IC_{50} of 0.68 ± 0.06 mg/mL. *Piper longum*-based Ag-NPs, though reported for antimicrobial activity, lacked quantified efficiency metrics such as entrapment efficiency or IC_{50} values [32]. These comparisons suggest that *A. polystachya* not only matches, but also in some cases outperforms other commonly used plants in terms of nanoparticle size, entrapment efficiency, and antioxidant potency, highlighting its potential as an efficient and sustainable reducing and stabilizing agent for nanomedicine applications.

Table 7. Entrapment efficiency of different formulation batches

Formulation Batches	(%EE)
F1	84.6
F2	69.1
F3	87.8
F4	**82.2**
F5	60.9
F6	86.5
F7	74.3
F8	74.7
F9	77.5
F10	79.6
F11	70.0
F12	80.2
F13	68.3
F14	65.3
F15	64.8
F16	75.5
F17	85.3
F18	88.0
F19	74.4
F20	52.9

SEM

The SEM analysis of the optimized silver nanoparticles functionalized with *A. polystachya* extract (AgNP-F) revealed crucial data about their morphology and size distribution. The nanoparticles exhibited a predominantly spherical shape, with diameters ranging from 39.7 to 90.7 nm. This narrow size range suggests a relatively uniform particle distribution, which is often desirable for various applications. The SEM images further provided visual evidence of the bio-components from the *A. polystachya* extract effectively capping the AgNPs, indicating successful functionalization. This capping is essential for stabilizing the nanoparticles and potentially enhancing their properties. Furthermore, the presence of

concentric rings observed in **Figure 12(A)** is a strong indicator of the high crystallinity of the AgNP-F. High crystallinity is often associated with improved physical and chemical properties of nanoparticles, such as enhanced optical, electrical, or catalytic characteristics. These findings from the SEM analysis provide valuable insights into the structural features of the optimized AgNP-F, which can inform their potential applications and further development.

The SEM histogram (**Figure 12B**) was quantitatively analyzed and revealed a particle size range of 200 nm to 1.5 µm with a mean size of 580 ± 120 nm. This confirms uniform, spherical morphology with minor agglomeration, supporting DLS and PXRD results and enhancing the reproducibility of the characterization.

PXRD

PXRD analysis (**Figure 13**) provided crucial insights into the structural characteristics of the optimized AgNP-F4 sample. The diffraction pattern revealed distinct peaks between 20° and 80° 2Θ, confirming the crystalline nature of the AgNPs. The XRD pattern displayed sharp diffraction peaks at 38.1°, 44.3°, 64.4°, and 77.4°, corresponding to the (111), (200), (220), and (311) planes of face-centered cubic AgNPs. Notably, the peak at 38.1° exhibited the highest intensity, indicating a preferential orientation or dominant crystal growth in this direction [33]. PXRD confirmed the crystalline nature of Ag-NPs with a crystallite size of ~10.4 nm, supported by SEM and DLS data.

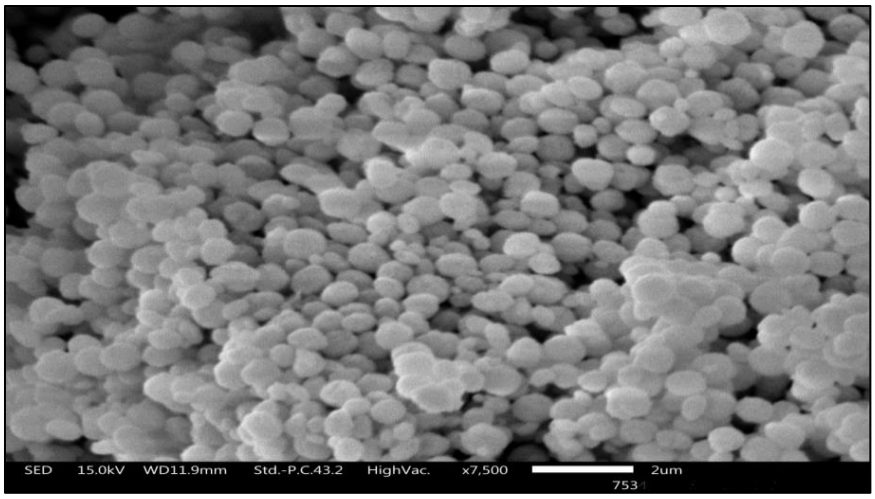

Figure 12(A). SEM image of F4 Ag-NP formulation

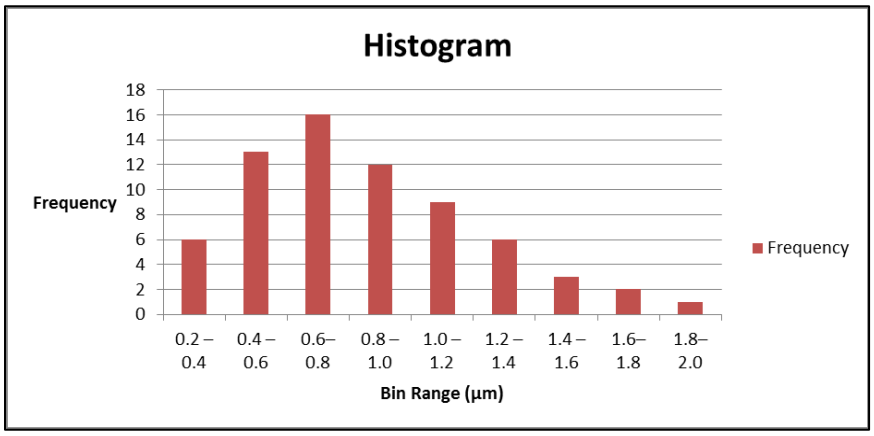

Figure 12(B). Particle size distribution form SEM image

The extract's crystalline components likely aided nanoparticle stabilization, confirming their structural integrity and biomedical potential. The sharpness and intensity of these peaks also provide data on the crystallite size and lattice strain in the AgNP-F4 sample. This comprehensive PXRD analysis not only confirms the successful synthesis of crystalline AgNPs, but also provides valuable data about their structural properties, which can be correlated with their potential applications and performance in various fields.

In vitro drug release study

The *in vitro* drug release study of batch F4 (AgNP-F) demonstrated superior performance, exhibiting the highest release rate of 93.38±2.96% among all tested formulations (**Table 8**, **Figure 14**). This evaluation was conducted using a dialysis method in phosphate-buffered saline (PBS) at pH 7.4, maintained at a physiological temperature of 37 ºC for 1 h. The amount of drug released was quantified using UV-Vis spectroscopy, a reliable and widely-used analytical technique for this purpose. The release profile was characterized by an initial burst release, which can be attributed to two primary factors: the small particle size of the AgNPs and the rapid diffusion of the drug from the outer shell of the nanoparticles. This burst release phenomenon is often observed in nanoparticle-based drug delivery systems and can be advantageous for achieving rapid therapeutic effects. The high release percentage and controlled release profile of batch F4 suggest its potential as an effective drug delivery system, warranting further investigation into its *in vivo* performance and therapeutic efficacy.

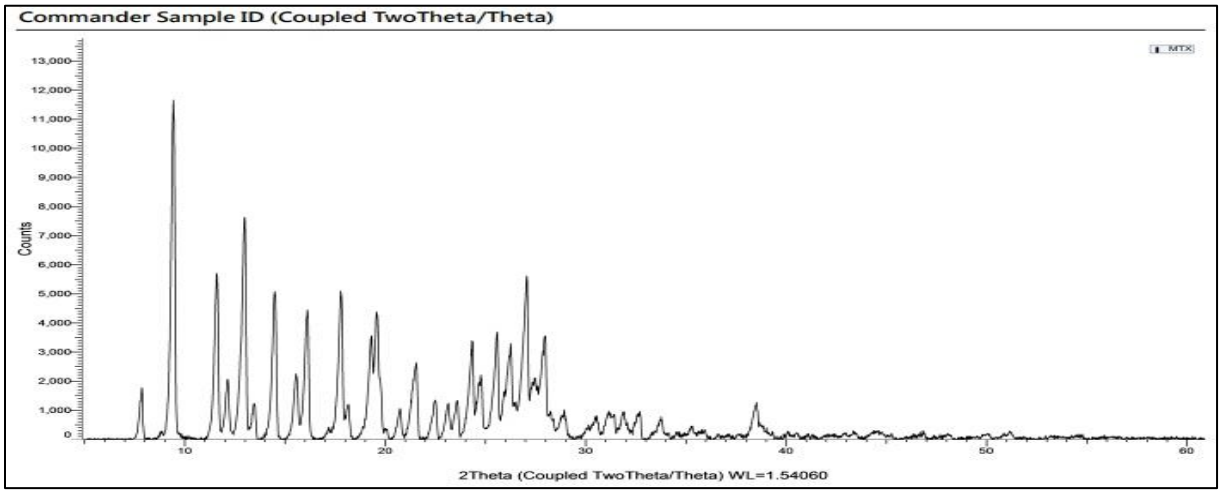

Figure 13. XRD Image of F4 Ag-NP formulation

Table 8. *In vitro* release profile of AgNP-F4

Table 8. *In vitro* release profile of AgNP-F4

Sr./ No.	Time (Hours)	AgNP-F (F4)
1	0	0
2	2	15.22±1.16
3	4	33.66±2.21
4	6	57.61±1.49
5	8	79.76±2.12
6	10	86.31±2.16
7	12	98.27±2.76

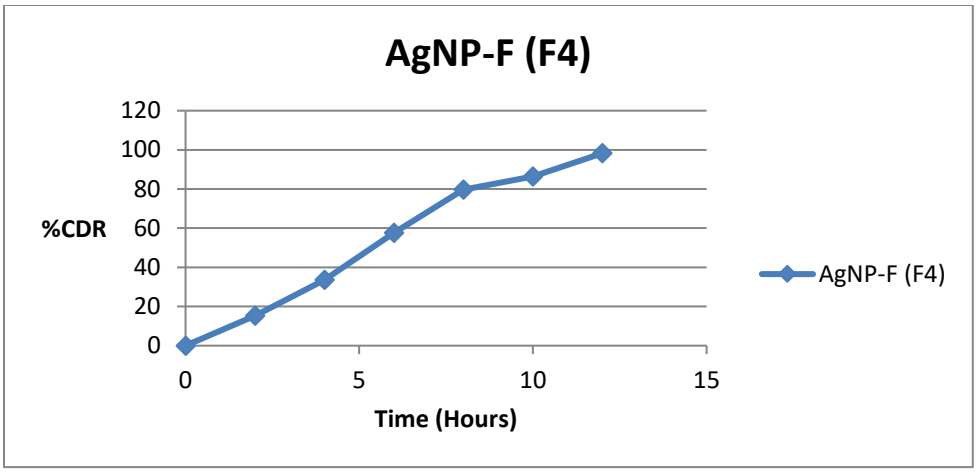

Figure 14. *In vitro* drug release study of Ag-NP-F4 formulation

Table 9. Stability study of parameters of the optimized formulation (F4)

Parameters	Initial Month	1st	2nd	3rd
%EE	82.20 ± 0.01	82.22 ± 0.04	82.40 ± 0.02	82.21 ± 0.03
Particle Size	39.7 ± 2.19	39.4 ± 2.20	39.9 ± 2.39	39.6 ± 2.14
PDI	0.189 ± 0.19	0.192 ± 0.25	0.188 ± 0.13	0.190 ± 0.26

Accelerated stability study

The accelerated stability study of the optimized AGNP-F (batch F4) demonstrated the remarkable consistency in key parameters over three months under the specified temperature and humidity conditions (**Table 9**).

The entrapment efficiency (%EE) remained highly stable, with only minor fluctuations observed. Initially at 82.20 ± 0.01%, it exhibited slight variations, reaching 82.40 ± 0.02% in the second month before settling at 82.21 ± 0.03% by the third month. Particle size, a critical factor in nanoparticle formulations, exhibited minimal changes throughout the study period. Starting at 39.7±2.19 nm, it remained within a narrow range, concluding at 39.6 ± 2.14 nm after three months. The polydispersity index (PDI), which indicates the uniformity of particle size distribution, also showed excellent stability. It began at 0.189 ± 0.19 and ended at 0.190 ± 0.26, demonstrating the formulation's capability to maintain a consistent particle size distribution over time. These results, as presented in **Table 9**, strongly suggest that the optimized AGNP-F formulation possesses robust stability characteristics, which is crucial for its potential pharmaceutical applications and shelf-life.

Antioxidant activity (DPPH)

The antioxidant activity of *A. polystachya* aqueous leaf extract and its synthesized Ag-NPs was evaluated using the DPPH assay (**Table 10**).

The extract showed a dose-dependent scavenging effect (18.65 ± 0.62% to 44.75 ± 1.91%) with an IC_{50} of 1.57 ± 0.07 mg/mL. In comparison, Ag-NPs exhibited stronger activity (44.87 ± 2.10% to 71.11 ± 2.68%) and a lower IC_{50} of 0.68 ± 0.06 mg/mL. Ascorbic acid showed the highest activity (IC_{50} = 0.35 ± 0.08 mg/mL). The enhanced antioxidant potential of the Ag-NPs is likely due to surface-bound phenolic compounds, which aid in silver ion reduction and contribute to nanoparticle stability and bioactivity [26,34-35].

The present study demonstrates the eco-friendly and sustainable synthesis of silver nanoparticles (Ag-NPs-F4) using *Aphanamixis polystachya* leaf extract as a natural reducing and stabilizing agent. Characterization confirmed the successful formation of stable, spherical Ag-NPs (10-50 nm) with a crystalline face-centered cubic structure.

Table 10. Antioxidant activity of *A. polystachya* aqueous leaf extract and its synthesized Ag-NPs (DPPH)

Samples	Concentration (mg/mL)	Scavenging Ability (%)	IC_{50} Value (mg/mL)
Aqueous Leaf Extracts	0.2	18.65±0.62	1.57±0.07
	0.4	24.78±1.12	
	0.6	29.45±1.47	
	0.8	36.85±1.55	
	1.0	44.75±1.91	
Ag-NPs	0.2	44.87±2.10	0.68±0.06
	0.4	51.46±2.42	
	0.6	59.11±3.21	
	0.8	63.65±2.10	
	1.0	71.11±2.68	
Ascorbic Acid Standard	0.2	51.45±1.05	0.35±0.08
	0.4	60.25±1.03	
	0.6	65.65±0.64	
	0.8	70.15±0.48	
	1.0	77.78±1.22	

These results are consistent with previously reported particle sizes using *Acalypha indica* (20-30 nm) [31] and *Olea europaea* (20-25 nm) leaf extracts [31]. FTIR analysis revealed the presence of proteins, flavonoids, and phenolic compounds, suggesting their involvement in nanoparticle formation and stabilization, while UV-Vis spectroscopy showed a surface plasmon resonance (SPR) peak at 425 nm. Further analyses using SEM, XRD, DLS, and zeta potential confirmed the nanoparticles' high purity, uniform size distribution, and stability. The antioxidant potential of both the Ag-NPs and crude extract was assessed via the DPPH assay. Ag-NPs exhibited significantly stronger free radical scavenging activity (IC_{50}=0.6 ± 0.068 mg/mL) compared to the crude extract (IC_{50}=1.57±0.07 mg/mL), likely due to the electron-donating and capping abilities of phenolic constituents. The Ag-NPs synthesized from *A. polystachya* exhibited strong antioxidant activity (IC_{50}=0.68 ±0.068 mg/mL), outperforming the crude extract and many plant-based Ag-NPs like those from *Piper longum*, which often lack quantified IC_{50} data [32]. Overall, the findings affirm the potent antioxidant activity of biosynthesized Ag-NPs derived from *A. polystachya*.

Conclusion

This study successfully demonstrated the green synthesis of silver nanoparticles (Ag-NPs) using *Aphanamixis polystachya* leaf extract, yielding highly stable and uniformly spherical nanoparticles with an optimized mean particle size of 39.7 nm and a zeta potential of -9.29 mV, indicating good colloidal stability. The crystalline nature of the Ag-NPs was confirmed via PXRD, showing sharp peaks corresponding to face-centered cubic structures, while FTIR spectra validated the involvement of phenolics, flavonoids, and proteins in nanoparticle stabilization and reduction. Among 20 formulations designed using Central Composite Design, formulation F4 achieved the best results, with an entrapment efficiency of 82.2% and an *in vitro* drug release rate of 98.27 ± 2.76% over 12 hours, making it an optimal candidate for drug delivery applications. Antioxidant assays revealed that Ag-NPs significantly outperformed the crude leaf extract, with an IC_{50} of 0.68 ± 0.06 mg/mL compared to 1.57 ± 0.07 mg/mL for the extract, highlighting nearly a 2.3-fold enhancement in free radical scavenging activity. This improved activity is attributed to surface-bound phytochemicals that contribute electron-donating properties and enhance bioavailability. These quantitative results confirm that *A. polystachya* serves as both an efficient reducing and capping agent, supporting its dual functional role in green synthesis. The high entrapment efficiency, sustained drug release, and potent antioxidant activity underscore the potential of these Ag-NPs for pharmaceutical and biomedical applications, such as targeted drug delivery, antioxidant

therapy, and wound healing. Moreover, the formulation exhibited excellent physicochemical stability over three months of accelerated storage, with negligible variation in particle size (±0.3 nm), PDI, and %EE, emphasizing its suitability for long-term applications. These findings position *A. polystachya*-mediated Ag-NPs as a sustainable and effective alternative to chemically synthesized nanoparticles. Future research should focus on *in vivo* pharmacokinetics, detailed mechanistic toxicology, and evaluation against disease models to fully harness the biomedical potential of these biogenic nanoparticles

Acknowledgments

None.

Conflict of Interest

There is no conflict of interest exists.

Orcid

P. Balaji
https://orcid.org/0000-0001-5317-1661

P. Shanmugasundaram
https://orcid.org/0000-0003-2961-0665

S. Umadevi
https://orcid.org/0000-0003-0242-2461

Mohd Masih Uzzaman Khan
https://orcid.org/0000-0002-2562-7403

I. Somasundaram
https://orcid.org/0000-0002-1598-0107

Rita Dadarao Chakole
https://orcid.org/0000-0003-2973-4473

Saravanan Govindaraj
https://orcid.org/0000-0002-1926-997X

References

[1]. M. Huston, M. DeBella, M. DiBella, A. Gupta, Green synthesis of nanomaterials, *Nanomaterials*, **2021**, *11*, 2130. [Crossref], [Google Scholar], [Publisher]

[2]. J. Singh, T. Dutta, K.H. Kim, M. Rawat, P. Samddar, P. Kumar, Green'synthesis of metals and their oxide nanoparticles: Applications for environmental remediation, *Journal of Nanobiotechnology*, **2018**, *16*, 1-24. [Crossref], [Google Scholar], [Publisher]

[3]. M.W. Ullah, S. Manan, W.A. Khattak, A. Shahzad, M. Ul-Islam, G. Yang, Biotemplate-mediated green synthesis and applications of nanomaterials, *Current Pharmaceutical Design*, **2020**, *26*, 5819-5836. [Crossref], [Google Scholar], [Publisher]

[4]. S. Ying, Z. Guan, P.C. Ofoegbu, P. Clubb, C. Rico, F. He, J. Hong, Green synthesis of nanoparticles: Current developments and limitations, *Environmental Technology & Innovation*, **2022**, *26*, 102336. [Crossref], [Google Scholar], [Publisher]

[5]. a) N. Koohzadi, Z. Rezayati Zad, A highly sensitive colorimetric determination of paraquat by silver nanoparticles, *Advanced Journal of Chemistry, Section B: Natural Products and Medical Chemistry*, **2021**, *3*, 311-322. [Crossref], [Google Scholar], [Publisher] b) S. Prabhu, E.K. Poulose, Silver nanoparticles: mechanism of antimicrobial action, synthesis, medical applications, and toxicity effects, *International Nano Letters*, **2012**, *2*, 1-10. [Crossref], [Google Scholar], [Publisher]

[6]. a) M. Alqaraleh, K.M. Khleifat, A. Al-Samydai, F.A. Al-Rawashde, B.O. Al-Najjar, F.G. Saqallah, Therapeutic potential of marine sponges and nanoparticles: A study on siphonochalina siphonella and AgNPs, *Journal of Medicinal and Pharmaceutical Chemistry Research*, **2025**, *7*, 745-761. [Crossref], [Google Scholar], [Publisher] b) X.F. Zhang, Z.G. Liu, W. Shen, S. Gurunathan, Silver nanoparticles: synthesis, characterization, properties, applications, and therapeutic approaches, *International Journal of Molecular Sciences*, **2016**, *17*, 1534. [Crossref], [Google Scholar], [Publisher]

[7]. a) I. Fareed Ali Karm, A. S. Dwaish, O.A.A. Dakhil, Algae extracts as reduction agents for biosynthesis of silver nanoparticles for alternative medicinal compounds, *Journal of Medicinal and Pharmaceutical Chemistry Research*, **2022**, *4*, 910-920. [Google Scholar], [Publisher] b) M.N. Owaid, Silver nanoparticles as unique nano-drugs, *Materials for Biomedical Engineering*, **2019**, 545-580. [Crossref], [Google Scholar], [Publisher]

[8]. A.C. Paiva-Santos, A.M. Herdade, C. Guerra, D. Peixoto, M. Pereira-Silva, M. Zeinali, F. Mascarenhas-Melo, A. Paranhos, F. Veiga, Plant-mediated green synthesis of metal-based nanoparticles for dermopharmaceutical and cosmetic applications, *International Journal of Pharmaceutics*, **2021**, *597*, 120311. [Crossref], [Google Scholar], [Publisher]

[9]. a) J.O. Igbalaye, A.G. Adeyemo, A.O. Adenubi, O. Ahmodu, B.O. Shodimu, F. Olasumbo Hazeez, S.A. Hassan, Silver nanoparticles synthesized using ageratum conyzoides leaf extract exhibit antioxidant, anti-inflammatory and α-glucosidase inhibitory properties, *Asian Journal of Green Chemistry*, **2024**, *8*, 25-38. [Crossref], [Google Scholar], [Publisher] b) F.A. Sheme, M.A. Aziz, M.R. Karim, M.H. Rahman, M.A. Rabbi, M. Nurujjaman, M.R. Habib, Green preparation of silver nanoparticles using leaf extract of Amoora rohituka for antioxidant, antibacterial and anticancer applications, *Journal of Agriculture and Food Research*, **2023**, *14*, 100889. [Crossref], [Google Scholar], [Publisher]

[10]. S. Shaikh, R. Dubey, S. Dhande, Y. Joshi, V.J. Kadam, Phytochemical and pharmacological profile of Aphanamixis polystachya: an overview, *Research Journal of Pharmacy and Technology*, **2012**, *5*, 1260-1263. [Crossref], [Google Scholar], [Publisher]

[11]. M.K. Gole, S. Dasgupta, Role of plant metabolites in toxic liver injury, *Asia Pacific Journal of Clinical Nutrition*, **2002**, *11*, 48-50. [Crossref], [Google Scholar], [Publisher]

[12]. K.V. Rakhesh, S.N. Ashalatha, K. Mahima, In vitro regeneration and chromatographic fingerprint analysis of Aphanamixis polystachya (Wall.) Parker by HPTLC technique, *South African Journal of Botany*, **2022**, *151*, 259-265. [Crossref], [Google Scholar], [Publisher]

[13]. Y. Rai, Growth and development of medicinal endangered tree species Aphanamixis polystachya (Wall.) Parker in District Meerut,(UP) India, *International Journal of Multidisciplinary and Current Research*, **2014**, *2*. [Google Scholar], [Publisher]

[14]. N.S. Alharbi, N.S. Alsubhi, A.I. Felimban, Green synthesis of silver nanoparticles using medicinal plants: Characterization and application, *Journal of Radiation Research and Applied Sciences*, **2022**, *15*, 109-124. [Crossref], [Google Scholar], [Publisher]

[15]. J.K. Sohal, A. Saraf, K.K. Shukla, Green synthesis of silver nanoparticles (ag-nps) using plant extract for antimicrobial and antioxidant applications: A review, *International Journal of Advanced Research in Science and Engineering*, **2017**, *6*, 766-777. [Google Scholar], [Publisher]

[16]. R. Gude, A.B. Joshi, A. Bhandarkar, A. Shirodker, S. Bhangle, Synthesis and characterisation of silver nanoparticles from the roots of aphanamixis polystachya, *World Jour of Pharm Research*, **2016**, *5*, 1399-1408. [Google Scholar], [Publisher]

[17]. P. Banerjee, M. Satapathy, A. Mukhopahayay, P. Das, Leaf extract mediated green synthesis of silver nanoparticles from widely available Indian plants: Synthesis, characterization, antimicrobial property and toxicity analysis, *Bioresources and Bioprocessing*, **2014**, *1*, 1-10. [Crossref], [Google Scholar], [Publisher]

[18]. A. Salayová, Z. Bedlovičová, N. Daneu, M. Baláž, Z. Lukáčová Bujňáková, Ľ. Balážová, Ľ. Tkáčiková, Green synthesis of silver nanoparticles with antibacterial activity using various medicinal plant extracts: Morphology and antibacterial efficacy, *Nanomaterials*, **2021**, *11*, 1005. [Crossref], [Google Scholar], [Publisher]

[19]. M.S. Alwhibi, D.A. Soliman, M.A. Awad, A.B. Alangery, H. Al Dehaish, Y.A. Alwasel, Green synthesis of silver nanoparticles: Characterization and its potential biomedical applications, *Green Processing and Synthesis*, **2021**, *10*, 412-420. [Crossref], [Google Scholar], [Publisher]

[20]. I.M. Chung, I. Park, K. Seung-Hyun, M. Thiruvengadam, G. Rajakumar, Plant-mediated synthesis of silver nanoparticles: their characteristic properties and therapeutic applications, *Nanoscale Research Letters*, **2016**, *11*, 1-14. [Crossref], [Google Scholar], [Publisher]

[21] R. Gude, A. B. Joshi, and A. Bhandarkar, Anti-oxidant, cytotoxic and apoptotic studies of root bark assisted silver nanoparticles from *Aphanamixis polystachya*, *International Journal of Research in Pharmaceutical Sciences*, **2019**, *10*, 943–950. [Crossref], [Publisher]

[22]. H. Shumail, S. Khalid, I. Ahmad, H. Khan, S. Amin, B. Ullah, Review on green synthesis of silver nanoparticles through plants, *Endocrine, Metabolic & Immune Disorders-Drug Targets (Formerly Current Drug Targets-Immune, Endocrine & Metabolic Disorders)*, **2021**, *21*, 994-1007. [Crossref], [Google Scholar], [Publisher]

[23]. R. Yadav, N.S. Chauhan, A.S. Chouhan, V. Soni, L. Omray, Antimicrobial screening of various extracts of Aphanmixis polystachya stems bark, *International Journal of Advances in Pharmaceutical Sciences*, **2010**, *1*. [Crossref], [Google Scholar]

[24]. V. Rungapamestry, A.J. Duncan, Z. Fuller, B. Ratcliffe, Changes in glucosinolate concentrations, myrosinase activity, and production of metabolites of glucosinolates in cabbage (Brassica oleracea var. capitata) cooked for different durations, *Journal of Agricultural and Food Chemistry*, **2006**, *54*, 7628-7634. [Crossref], [Google Scholar], [Publisher]

[25]. A. Qazi, J. Pal, M.i. Maitah, M. Fulciniti, D. Pelluru, P. Nanjappa, S. Lee, R.B. Batchu, M. Prasad, C.S. Bryant, Anticancer activity of a broccoli derivative, sulforaphane, in barrett adenocarcinoma: potential use in chemoprevention and as adjuvant in chemotherapy, *Translational oncology*, **2010**, *3*, 389-399. [Crossref], [Google Scholar], [Publisher]

[26]. D. Philip, Mangifera indica leaf-assisted biosynthesis of well-dispersed silver nanoparticles, *Spectrochimica Acta Part A: Molecular and Biomolecular Spectroscopy*, **2011**, *78*, 327-331. [Crossref], [Google Scholar], [Publisher]

[27]. T. Mustapha, N. Misni, N.R. Ithnin, A.M. Daskum, N.Z. Unyah, A review on plants and microorganisms mediated synthesis of silver nanoparticles, role of plants metabolites and applications, *International Journal of Environmental Research and Public Health*, **2022**, *19*, 674. [Crossref], [Google Scholar], [Publisher]

[28]. S. Ahmed, M. Ahmad, B.L. Swami, S. Ikram, A review on plants extract mediated synthesis of silver nanoparticles for antimicrobial applications: A green expertise, *Journal of Advanced Research*, **2016**, *7*, 17-28. [Crossref], [Google Scholar], [Publisher]

[29]. S. Agarwal, A.K. Dutta, Revolutionizing Drug Development: The role of AI in modern pharmaceutical research, *Bioinformatics and Beyond, CRC Press*, 206-227. [Google Scholar], [Publisher]

[30]. V. Sakaray, Y.S. Rao, N.V. Naidu, Green Synthesis of Silver Nanoparticles by Acalypha indica Plant Extract and Their Approach towards Multifunctional Applications, *Nano Biomedicine & Engineering*, **2024**, *16*. [Crossref], [Google Scholar], [Publisher]

[31]. A.I. Felimban, N.S. Alharbi, N.S. Alsubhi, Optimization, characterization, and anticancer potential of silver nanoparticles biosynthesized using Olea europaea, *International Journal of Biomaterials*, **2022**, *2022*, 6859637. [Crossref], [Google Scholar], [Publisher]

[32]. H. Huang, K. Shan, J. Liu, X. Tao, S. Periyasamy, S. Durairaj, Z. Jiang, J.A. Jacob, Synthesis, optimization and characterization of silver nanoparticles using the catkin extract of Piper longum for bactericidal effect against food-borne pathogens via conventional and mathematical approaches, *Bioorganic Chemistry*, **2020**, *103*, 104230. [Crossref], [Google Scholar], [Publisher]

[33]. K. Jurkiewicz, M. Kamiński, A. Bródka, A. Burian, Atomistic origin of nano-silver paracrystalline structure: molecular dynamics and x-ray diffraction studies, *Journal of Physics: Condensed Matter*, **2022**, *34*, 375401. [Crossref], [Google Scholar], [Publisher]

[34]. K. Shimada, K. Fujikawa, K. Yahara, T. Nakamura, Antioxidative properties of xanthan on the autoxidation of soybean oil in cyclodextrin emulsion, *Journal of Agricultural and Food Chemistry*, **1992**, *40*, 945-948. [Crossref], [Google Scholar], [Publisher]

[35]. S. Saumya, P.M. Basha, Antioxidant effect of Lagerstroemia speciosa Pers (Banaba) leaf extract in streptozotocin-induced diabetic mice, *Indian Journal of Experimental Biology*, **2011**. [Google Scholar], [Publisher]